

This is the **accepted version** of the journal article:

Francàs Forcada, Laia; Richmond, Craig; Garrido Barros, Pablo; [et al.].
«Ru-bis(pyridine)pyrazolate (bpp)-Based Water-Oxidation Catalysts Anchored
on TiO₂ : The Importance of the Nature and Position of the Anchoring
Group». Chemistry, Vol. 22, Issue 15 (April 2016), p. 5261-5268. DOI
10.1002/chem.201504015

This version is available at <https://ddd.uab.cat/record/289044>

under the terms of the  **IN**
COPYRIGHT license

Ru-bpp-based Water Oxidation Catalysts Anchored on TiO₂: The Importance of the Nature and Position of the Anchoring Group

Laia Francàs,^[a] Craig Richmond,^[a] Pablo Garrido-Barros,^[a] Nora Planas,^[a] Stephan Roeser,^[a] Jordi Benet-Buchholz,^[a] Lluís Escriche,^[b] Xavier Sala,^[b] Antoni Llobet ^{*,[a,b]}

Dedication ((optional))

Abstract: Three distinct functionalization strategies have been applied to the $\text{in},\text{in}-[\{\text{Ru}^{\text{II}}(\text{trpy})\}_2(\mu\text{-bpp})(\text{H}_2\text{O})_2]^{3+}$ water oxidation catalyst framework to form new derivatives capable of adsorbing onto titania substrates. Firstly, a terpyridine-based ligand functionalized with sulfonate groups (4'-(p-tolyl)-2,2':6',2''-terpyridine = trpy-S_a) was prepared and characterized. A second terpyridine-based ligand, functionalized with a phosphonate group (phosphonic acid P-[2,2':6',2''-terpyridin]-4'-yl-diethyl ester = trpy-P_e), was also selected and both ligands were then used to synthesize ruthenium complexes of general formula $\text{in},\text{in}-[\{\text{Ru}^{\text{II}}(\text{trpy-X})\}_2(\mu\text{-bpp})(\text{L-L})]^{n+}$. Finally, a post-complexation ligand modification strategy was used to create a tetranuclear ruthenium dyad, $\text{in},\text{in}-[\{\text{Ru}^{\text{II}}(\text{trpy})\}_2(\mu\text{-R}_2\text{bpp})(\text{L-L})]^{n+}$, where $\text{R} = \{(\text{O-Phen})\text{Ru}(\text{dcbpy})_2\}$. The complexes were characterized in solution by 1D and 2D NMR spectroscopy, UV-Vis spectroscopy and electrochemical techniques. The complexes were then anchored on TiO₂ coated FTO films and the reactivity of these new materials as water oxidation catalysts was tested electrochemically through controlled potential electrolysis (CPE) with oxygen evolution detected by headspace analysis with a Clark electrode. The electrochemical properties of the heterogenized complexes were significantly modified with regard to those of their corresponding homogenous counterparts, which in turn had a direct implication on their performance as water oxidation catalysts. DFT calculations for the anchored catalysts were performed in conjunction with the experimental techniques to deduce the possible reasons for this change in behaviour.

Introduction

Artificial Photosynthesis (AP) has the potential to fulfil our future energy demands through the direct generation of inexhaustible solar fuels such as hydrogen and methanol from the solar-assisted splitting of water.^[1] The key to unlocking the potential of this approach, however, lies not only in the reduction of CO₂ and H⁺ to their useful counterparts, e.g. CH₄, MeOH and H₂, but also in releasing the electrons required for these steps from water. Any design for a photocatalytic water splitting device or cell will therefore need to incorporate a water oxidation catalyst, a substrate reduction catalyst and a photoactive component(s).^[2] The independent scrutiny of the individual device components has proved to be a useful strategy for their analysis and optimization and many advances have been made on all fronts over the last few years.^[3,4] A popular approach to creating a functional photoanode for a water splitting device involves the anchoring of catalysts and/or dyes (or precombined dyads) on semiconductor materials such as TiO₂.^[4] Several groups have been particularly active in this area and have produced some very active electrodes using this approach.^[4,5]

The $\text{in},\text{in}-[\{\text{Ru}^{\text{II}}(\text{trpy})\}_2(\mu\text{-bpp})(\text{H}_2\text{O})_2]^{3+}$ water oxidation catalyst ($\text{trpy} = 2,2':6',2''\text{-terpyridine}$; $\text{bpp} = \text{Bispyridinepyrazolate}$,^[6] has previously been immobilized through the electropolymerization of a pyrrole-modified Ru-bpp system onto different conducting electrodes (Vitreous Carbon Sponge and Fluorinated Tin Oxide, FTO),^[7] however, despite the observed increase in robustness when compared with its homogeneous counterpart, catalyst deactivation was still observed due to oxidation of the polypyrrole backbone during the catalytic process. Subsequent attempts were made to anchor the catalyst on more robust substrates like TiO₂, SiO₂ and Nafion but this did not result in robust water oxidation anodes due to oxidative ligand degradation and catalyst leaching.^[8,9]

[a] Dr. Laia Francàs, Dr. Craig Richmond, Pablo Garrido-Barros, Dr. Nora Planas, Dr. Stephan Roeser, Dr. Jordi Benet-Buchholz, Prof. Dr. Antoni Llobet
Institute of Chemical Research of Catalonia (ICIQ)
Av. Països Catalans 16, E-43007 Tarragona, Spain
E-mail: allobet@iciq.es
[b] Dr. Xavier Sala, Dr. Lluís Escriche, Prof. Dr. Antoni Llobet
Departament de Química, Universitat Autònoma de Barcelona,
Cerdanyola del Vallès, 08193 Barcelona, Spain.

Supporting information for this article is given via a link at the end of the document. ((Please delete this text if not appropriate))

In this work three new strategies based on three distinct ligand architectures are presented for the modification and anchoring of Ru-bpp-type catalysts on titania: (i) 5-([2,2':6',2''-terpyridin]-4'-yl)-2-methylbenzene-1,3-disulfonate (**4**, trpy-S_a in Scheme 1.); (ii) Phosphonic acid, P-[2,2':6',2''-terpyridin]-4'-yl-diethyl ester (**2**, trpy-P_e in Scheme 1.); and (iii) Bis-chloropyridinepyrazolate (**6**, bcp in Chart 1.) Ligands **4** and **6** are reported here for the first time whilst **2** was purchased from HetCat (Switzerland). Complexation to ruthenium salts followed by post-synthetic manipulation allowed the formation of a series of novel Ru-bpp-type catalysts of the general formula $\text{in, in-}[\{\text{Ru}^{\text{II}}(\text{trpy-R}_1)\}_2(\mu\text{-R}_2\text{bpp})(\text{L-L})]^n+$, where $\text{R}_1 = \text{S}_a, \text{P}_e, \text{P}_a$, or H; $\text{R}_2 = (\text{O-Phen})\text{Ru}(\text{dcbpy})_2$ or H; and $\text{L} = \mu\text{-PhCOO}, \mu\text{-AcO}, \mu\text{-Cl}, \mu\text{-Br}$, or H_2O (See Scheme 1.). The complexes were characterized by 1D and 2D NMR spectroscopy, UV/Vis spectroscopy and electrochemical techniques and then anchored on TiO_2 coated FTO films. The reactivity of the new materials as water oxidation catalysts was assessed electrochemically through controlled potential electrolysis (CPE) with oxygen evolution detected by headspace analysis with a Clark electrode.

Results and Discussion

Synthesis of Ligands and Complexes (Chart 1 and Schemes 1 and 2). Treatment of commercial 4'-(p-tolyl)-2,2':6',2''-terpyridine with concentrated H_2SO_4 yielded the 5-([2,2':6',2''-terpyridin]-4'-yl)-2-methylbenzene-1,3-disulfonate ligand (**4**, trpy-S_a). The intermediate $[\text{RuCl}_3(\text{trpy-S}_a)]$, **9**, was then prepared by drop-wise addition of a highly diluted ethanol solution of **4** to a refluxing solution of ruthenium trichloride in ethanol saturated with LiCl, precipitating the desired complex upon cooling. Reaction of **9** with

the dinucleating Hbpp ligand **5** in the presence of NEt_3 generated a mixture of dinuclear and mononuclear Ru complexes. Reverse phase (C18) chromatography, eluting with methanol and a sodium acetate/acetic acid buffer solution (pH = 4), allowed the direct isolation of the acetato-bridged complex as its disodium salt **Na₂[12a]**, $[\{\text{Ru}^{\text{II}}(\text{trpy-S}_a)\}_2(\mu\text{-bpp})(\mu\text{-AcO})]\text{Na}_2$.

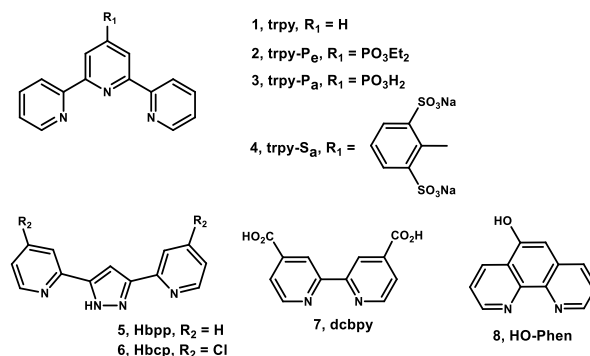
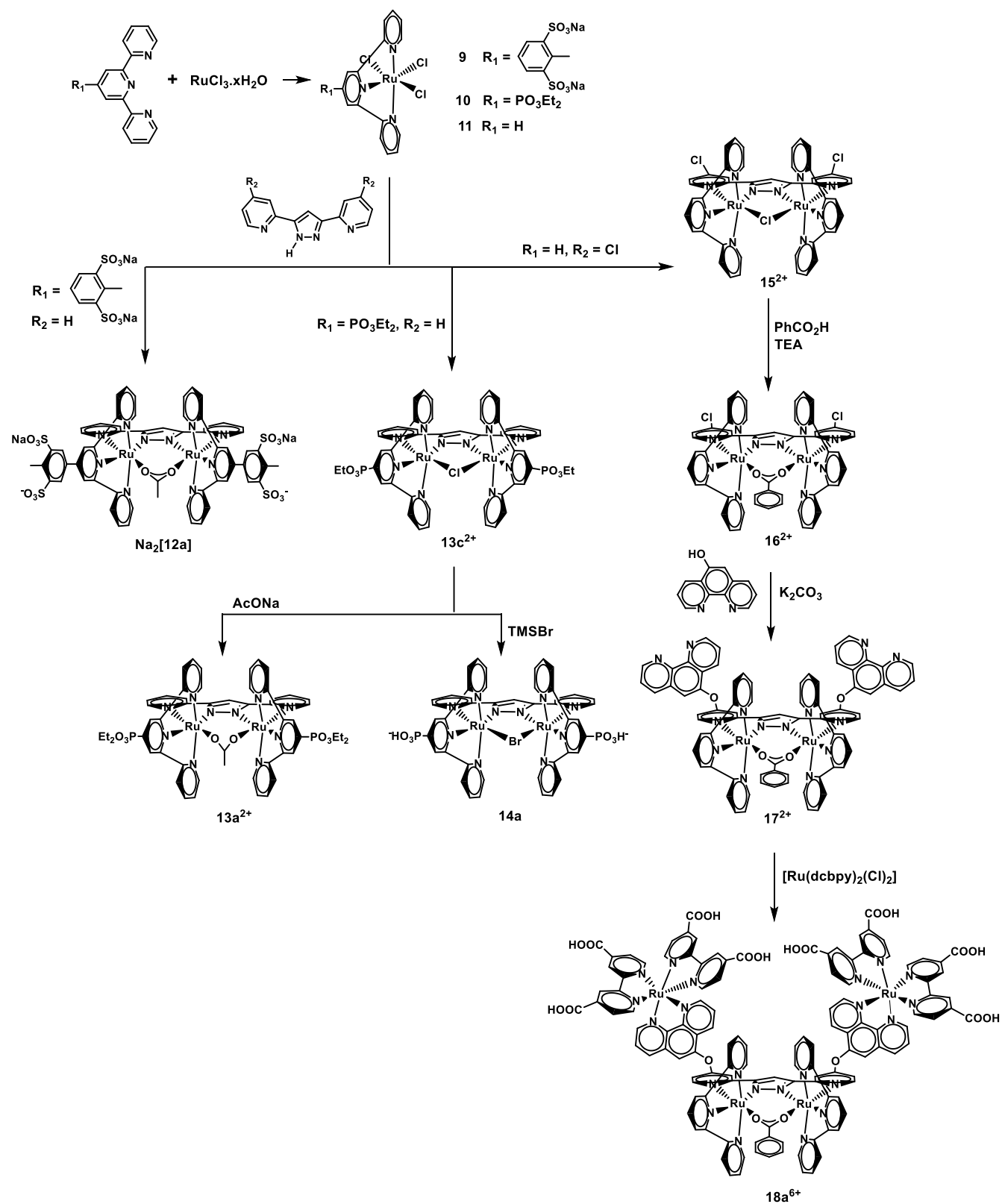


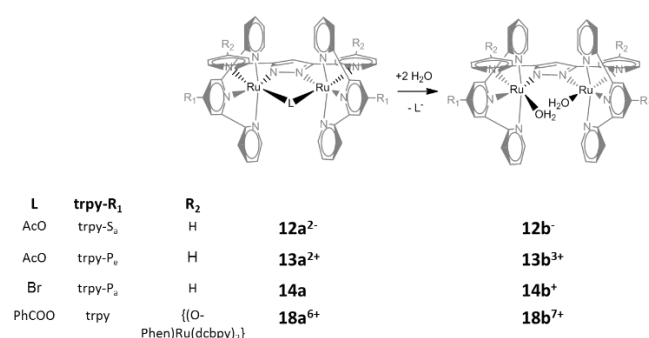
Chart 1. Structures and abbreviations of the ligands used in this work.

The ester form of the trpy-P_a ligand, trpy-P_e, **2**, was used to synthesize the corresponding ruthenium complexes due to the lower coordination capacity of the ester group, which minimized the generation of undesired compounds. Furthermore, working with the ester derivative instead of the phosphonic acid allowed a simpler workup procedure because of its higher solubility in organic solvents. The reaction between ruthenium trichloride and trpy-P_e gave $[\text{RuCl}_3(\text{trpy-P}_e)]$, **10**, which again could be reacted with the Hbpp ligand, however, in this case the dinuclear chloro-bridged complex, $[\{\text{Ru}^{\text{II}}(\text{trpy-P}_e)\}_2(\mu\text{-bpp})(\mu\text{-Cl})](\text{PF}_6)_2$, **[13c](PF₆)₂**, could be isolated. Refluxing with an excess of acetate salt allowed clean conversion to the acetato-bridged complex, $[\{\text{Ru}^{\text{II}}(\text{trpy-P}_e)\}_2(\mu\text{-bpp})(\mu\text{-OAc})](\text{PF}_6)_2$, **[13a](PF₆)₂**.



Scheme 1. Synthetic routes towards complexes, **Na₂[12a]**, **13a²⁺**, **14a** and **18a⁶⁺**.

The acetato-bridged complexes **12a**²⁻ and **13a**²⁺ are excellent pre-catalysts as they are easy to handle crystalline materials that can be obtained in relatively high yields yet are still easily converted to the active bis-aquo derivatives due to the lability of the acetato-bridge in acidic media (See Scheme 2).^[6] The hydrolysis of the phosphonate ester groups of **[13c](PF₆)₂** is carried out under strictly anhydrous conditions to obtain the phosphonic acid derivative, **[{Ru^{II}(trpy-P_a)₂(μ-bpp)(μ-Br)]**, **14a**. During the hydrolysis, the chloro-bridge is replaced by a bromo-bridging group and the complex precipitates in its charge neutral form. This was confirmed by X-ray diffraction (XRD) analysis (Figure 1), MS (Figure S37) and redox titration (Figure S31).



Scheme 2. Hydrolysis of bridged complexes **a** to bis-aquo complexes **b** and complex labelling scheme.

Crystals of **14a** suitable for XRD analysis were obtained by slow evaporation of a MeOH solution. The crystallographic data are listed in Table S1 in the ESI and a view of its molecular structure is depicted in Figure 1. The structure shows the two ruthenium centers with a distorted octahedral coordination and doubly bridged by the bpp and the bromo ligands that occupy three of the four meridional coordination positions. The fourth position is occupied by the tridentate trpy ligand, which is oriented perpendicular to the bpp. The added phosphonic acid group causes a distortion in the planarity of the terpyridine group, the angle between the two trpy ligands closing to 47° instead of the 66° found for the non-substituted Cl-bridge complex **[{Ru^{II}(trpy)₂(μ-bpp)(μ-Cl)](PF₆)₂**.^[6] This angle diminution could be caused by the hydrogen bonds established between the two phosphonic acid groups and a disordered methanol molecule situated in-between (Figure 1b and ESI, CCDC numbers, 1429405-1429407). As expected, the phosphonic acid moiety attached to the central pyridine of the terpyridine is not involved in the first coordination sphere of ruthenium. The metal-ligand

bond distances are typical and similar to the values obtained for related ruthenium complexes.^[6-11]

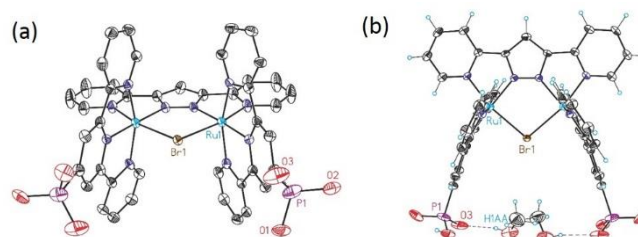


Figure 1. ORTEP (50% probability) for complex **14a**. (a) Frontal view. Hydrogen atoms are not shown. (b) Upper view showing the contact of a disordered methanol molecule and the two phosphonate groups. Color codes: Ru, light blue; Br, Brown; N, dark blue; O, red; H, white; P, purple; C, black..

The tetranuclear complex, **[{Ru^{II}(trpy)₂(μ-((O-Phen)Ru^{II}(dcbpy)₂bpp)(μ-PhCOO))](PF₆)₆**, **[18a](PF₆)₆**, was synthesized in 3 steps from the dinuclear complex, **[{Ru^{II}(trpy)₂(μ-bcp)(μ-Cl)](PF₆)₂**, **[15](PF₆)₂** (See Scheme 2). Compound **[15](PF₆)₂** was prepared using the same methodology used for compound **[13c](PF₆)₂** except the Hbcp ligand was replaced with the bis-chlorinated version, Hbcp, **6**. The bridging chloro ligand was hydrolyzed and replaced with a base-stable bridging benzoate to give **[{Ru^{II}(trpy)₂(μ-bcp)(μ-PhCOO))](PF₆)₂**, **[16](PF₆)₂**, and then a Wilkinson-style ether formation was used to substitute the chloro groups of the bcp ligand with 5-hydroxy-1,10-phenanthroline (HO-phen) to give complex **[{Ru^{II}(trpy)₂(μ-(Phen-O)₂bpp)(μ-PhCOO))](PF₆)₂**, **[17](PF₆)₂**. Finally the dinuclear complex containing the pendant phenanthrolines, **[17](PF₆)₂**, was reacted with (dcbpy)₂RuCl₂ (dcbpy = [2,2'-bipyridine]-4,4'-dicarboxylic acid) to give the tetranuclear Ru complex **[18a](PF₆)₆** after acidification and precipitation, which has been characterized by NMR, electrochemical techniques and elemental analysis (experimental section and Figures S10, S22 and S30).

Anchoring of complexes on TiO₂. Compounds **12a**²⁻, **14a** and **18a**⁶⁺ were anchored onto the surface of a mesoporous TiO₂ film, previously prepared *via* doctor blading of a TiO₂ paste onto a conductive FTO covered glass slide. The general procedure consisted of soaking the bare FTO-TiO₂ films in a solution containing the complex to be anchored. The nature of the different anchoring groups and modifications resulted in very different solubility properties for the three complexes, distinct solvents were therefore used for anchoring in each case. The anchoring of

the complexes was confirmed and quantified spectroscopically and electrochemically (see Figures 2, 3).

For compound **12a**²⁻ containing the trpy-S_a ligand, the μ -acetato complex **12a**²⁻ was first dissolved in a pH = 2 aqueous nitric acid solution, which in a short time leads to the complete hydrolysis of the acetate-bridge to afford the bis-aquo complex **12b**⁻ (Scheme 2). The TiO₂ covered FTO films were then soaked in the acidic solution and the resulting pH was readjusted to 2 if required. The sensitization process of the FTO-TiO₂ films was followed by consecutive registering of the UV-vis spectra of the acidic solution over time, around 48h were required for maximum sensitization.

The phosphonated compound **14a** was dissolved in methanol to get a 0.135 mM solution wherein the FTO-TiO₂ plate was soaked. The carboxylated dyad **18a**⁶⁺ was anchored onto the FTO-TiO₂ electrodes by soaking the electrode plates in a 0.03 mM solution of [**18a**](PF₆)₆ in a 1:1 mixture of DMF and EtOH for 16 hours. The band appearing between 430 and 530 nm in the UV-vis spectra, attributed to the MLCT for this type of complexes, confirmed the attachment of the complex to the FTO-TiO₂ surface (Figure 2). For the anchoring of **12b**⁻, the analysis was more thorough in order to identify the exact nature of the anchored species due to the use of water as anchoring solvent. When the visible region of the UV-vis spectra for compound TiO₂-**12b** and **12b**⁻ in water at pH = 1 (triflic acid) are overlaid, the two characteristic MLCTs bands are almost equal (Figure 2a). Only a very slight red shift is observed for the adsorbed compound, which is consistent with observations made for other TiO₂-adsorbed compounds reported.^[12] When considering the possibility of anchoring occurring *via* coordination of the surface hydroxyls of the TiO₂ to the Ru metal centers, a significant red shift on the resulting spectra would be expected. The lack of a large red shift therefore suggests the bis-aquo compound anchors to the TiO₂ through the sulfonate groups and not through any undesired interaction between the surface hydroxyls and the Ru centers.

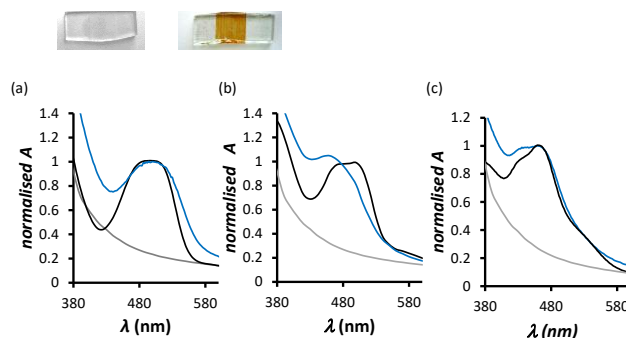
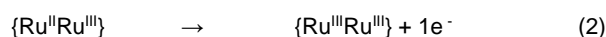
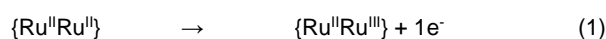


Figure 2. Top: Picture of a FTO-TiO₂ film before (left) and after (right) the anchoring process. Bottom: UV-Vis spectra for; (a) grey, TiO₂ blank; blue, TiO₂-**12b**; and black, **12b**⁻ in a triflic acid solution (pH = 1); (b) grey, TiO₂ blank; blue, TiO₂-**14a** and black, **14a** in MeOH; and (c) grey, TiO₂ blank; blue, TiO₂-**18a** and black, **18a**⁶⁺ in Ethanol.

The anchored bis-aquo-complexes TiO₂-**14b** and TiO₂-**18b** were obtained by soaking the TiO₂-**14a** and TiO₂-**18a** electrodes in 0.1 M triflic acid aqueous solution (pH=1) over a period of 24 h. No desorption was observed when the final acidic solution was analysed by UV-vis spectroscopy and electrochemical techniques.

Electrochemistry. The dinuclear Ru-bpp complexes containing the carboxylato and halo bridges all present two consecutive 1e⁻ oxidations that correspond to the processes represented in equations 1-2 (see also Figure 3 and Table 1.). The ca. 300-400 mV difference observed between the Ru(II,III/II,II) and Ru(III,III/II,III) redox processes is indicative of electronic coupling between the metal centers through the bridging ligands.



The tetranuclear dyad [**18a**](PF₆)₆ contains two consecutive 1e⁻ oxidations that correspond to the same redox processes represented in equations 1-2, similar to the other dinuclear compounds, but also has an additional 2e⁻ oxidation that corresponds to the simultaneous 1e⁻ oxidation of each of the photosensitizer ruthenium centres (See Figure 3c and Table 1 entry 13).

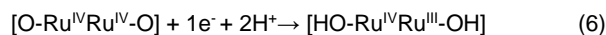
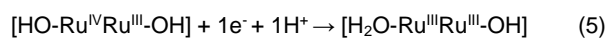
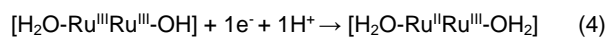
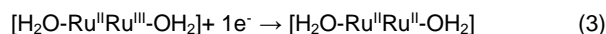
Substitution of the terpyridine ligands does have an effect on the redox potentials of the complexes, with a difference of up to 120 mV observed for the first redox couple of the phosphonate ester

complex **[13a](PF₆)₂** and the non-substituted trpy complex (see Table 1, entries 2 and 7). The second redox couple is not as significantly affected as the first couple with a difference of only 70 mV. Similar electronic effects can also be observed due to substitution of the bpp ligand but the shift in potentials is less pronounced, for example when one compares the electron withdrawing chloro groups and electron donating phenanthroline-ether groups of compounds **16** and **17** (Table 1 entries 2, 11 and 12).

Once anchored on TiO₂, the bridged-complexes **[18a](PF₆)₆** and **14a** retain the electrochemical characteristics observed prior to anchoring (Figures 3b, c, d and e and Table 1 entries 9, 13, 15 and 17).

The redox behavior of the bis-aquo complexes is radically different to the previously described bridged-complexes because

the electron transfer can be coupled to proton transfer (PCET). A typical CV of the aquo compound **12b⁻** in a 0.1M triflic acid solution (pH=1) is presented in Figure S16. This CV of compound **12b⁻** differs very little from that of the widely studied unmodified bpp-aquo system when registered in the same conditions ^[13] therefore the four waves observed for **12b⁻** could be tentatively assigned, as depicted in Equations 3-6. It is also important to note the presence of an electrocatalytic wave beginning at around 1.3 V vs SSCE, which corresponds to the catalytic oxidation of water.



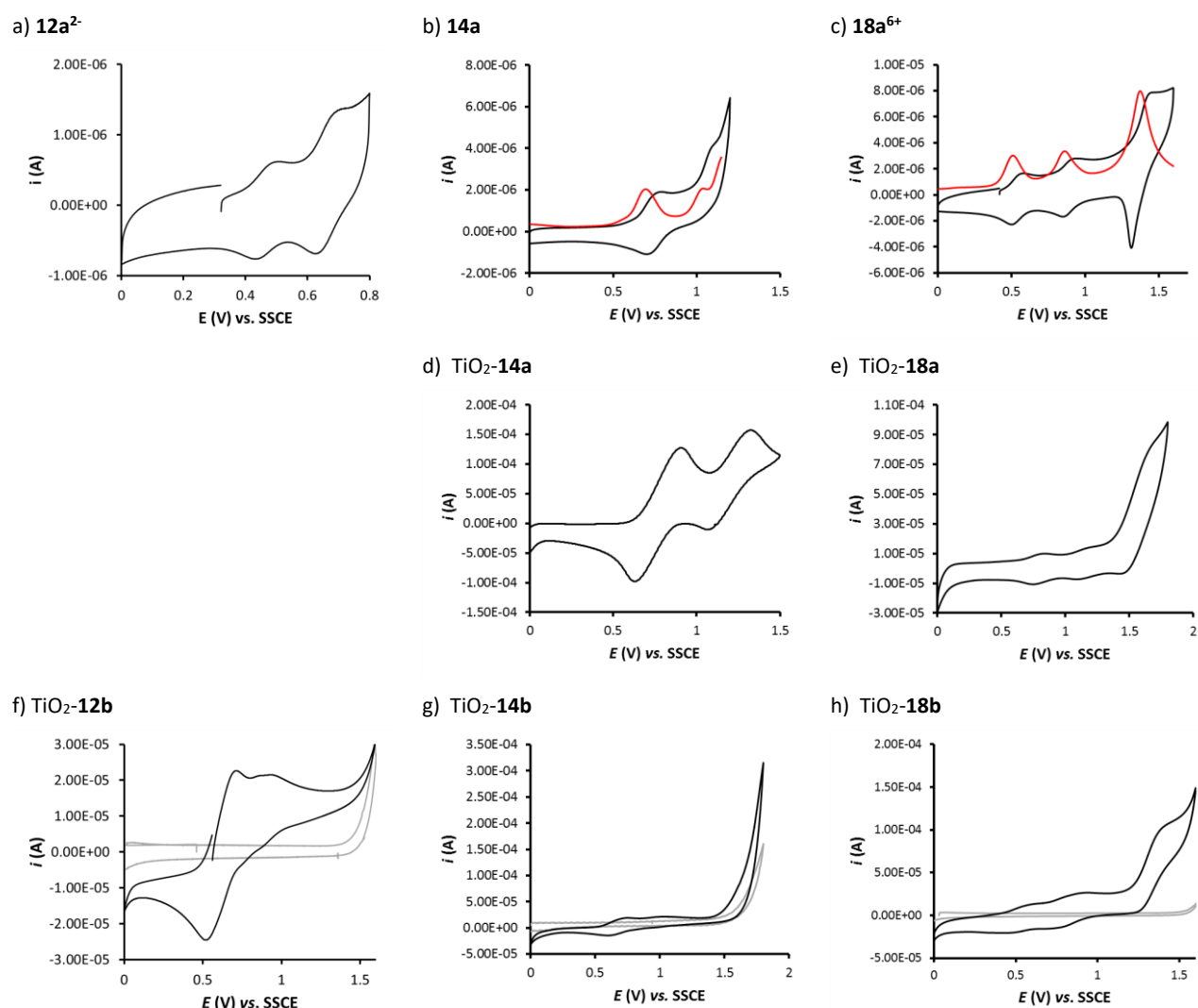


Figure 3. a) CV in 0.1M TBAH in MeOH for complex **12a²⁻**; b) CV (black) and DPV (red) in 0.1M TBAH in MeOH for complex **14a**; c) CV (black) and DPV (red) in 0.1M TBAH in DCM for complex **18a⁶⁺**; d) CV for **TiO₂-14a** in 0.1 M TBAH in DCM; e) CV for **TiO₂-18a** in 0.1M TBAH in DCM; f) CV for **TiO₂-12b** (black) compared to a bare FTO@TiO₂ plate (grey) in 0.1 M triflic acid (pH = 1); g) CV for **TiO₂-14b** (black) compared to a bare FTO@TiO₂ plate (grey) in 0.1 M triflic acid (pH = 1); h) CV for **TiO₂-18b** (black) compared to a bare FTO@TiO₂ plate (grey) in 0.1 M triflic acid (pH = 1). The **TiO₂-12a** CV in organic solvent was not recorded because the compound was directly anchored in the aquo form.

Table 1. Redox properties for the complexes described in this work and for related Ru-bpp complexes for comparative purposes. ($E_{1/2}$ in V vs. SSCE).

| Entry | Complex | | III-II/II-II E _{1/2} | III-III/III-II E _{1/2} | III-IV/III-III E _{1/2} | III/II (PS) E _{1/2} |
|-------------------|--|-----------------------|----------------------------------|------------------------------------|------------------------------------|---------------------------------|
| 1 ^[a] | [{Ru ^{II} (trpy)} ₂ (μ-bpp)(μ-Cl)] ²⁺ | | 0.71 | 1.12 | | |
| 2 ^[a] | [{Ru ^{II} (trpy)} ₂ (μ-bpp)(μ-AcO)] ²⁺ | | 0.73 | 1.05 | | |
| 3 ^[b] | [{Ru ^{II} (trpy)} ₂ (μ-bpp)(H ₂ O) ₂] ³⁺ | | 0.59 | 0.65 | 0.88 | |
| 4 ^[d] | [{Ru ^{II} (trpy-S _a)} ₂ (μ-bpp)(μ-AcO)] ²⁻ | 12a | 0.65 | 0.95 | | |
| 5 ^[b] | [{Ru ^{II} (trpy-S _a)} ₂ (μ-bpp)(H ₂ O) ₂] ¹⁻ | 12b | 0.55 | 0.64 | 0.87 | |
| 6 ^[a] | [{Ru ^{II} (trpy-P _e)} ₂ (μ-bpp)(μ-Cl)] ²⁺ | 13c | 0.84 | 1.19 | | |
| 7 ^[a] | [{Ru ^{II} (trpy-P _e)} ₂ (μ-bpp)(μ-AcO)] ²⁺ | 13a | 0.85 | 1.12 | | |
| 8 ^[c] | [{Ru ^{II} (trpy-P _e)} ₂ (μ-bpp)(H ₂ O) ₂] ³⁺ | 13b | 0.66 | 0.70 | 0.95 | |
| 9 ^[d] | [{Ru ^{II} (trpy-P _a)} ₂ (μ-bpp)(μ-Br)] | 14a | 0.69 | 1.03 | | |
| 10 ^[a] | [{Ru ^{II} (trpy)} ₂ (μ-bcp)(μ-Cl)] ²⁺ | 15 | 0.77 | 1.16 | | |
| 11 ^[a] | [{Ru ^{II} (trpy)} ₂ (μ-bcp)(μ-PhCOO)] ²⁺ | 16 | 0.70 | 1.10 | | |
| 12 ^[a] | [{Ru ^{II} (trpy)} ₂ (μ-(O-Phen) ₂ bpp)(μ-PhCOO)] ²⁺ | 17 | 0.68 | 1.01 | | |
| 13 ^[e] | [{Ru ^{II} (trpy)} ₂ (μ-((O-Phen)Ru ^{II} (dcbpy) ₂) ₂ bpp)(μ-PhCOO)] ⁶⁺ | 18a | 0.51 | 0.86 | | 1.38 |
| 14 ^[b] | TiO ₂ -[{Ru ^{II} (trpy-S _a)} ₂ (μ-bpp)(H ₂ O) ₂] ³⁻ | TiO ₂ -12b | 0.56 | 0.61 | 0.81 | |
| 15 ^[d] | TiO ₂ -[{Ru ^{II} (trpy-P _a)} ₂ (μ-bpp)(μ-Br)] | TiO ₂ -14a | 0.77 | 1.20 | | |
| 16 ^[b] | TiO ₂ -[{Ru ^{II} (trpy-P _a)} ₂ (μ-bpp)(H ₂ O) ₂] ²⁺ | TiO ₂ -14b | 0.60 | 0.63 | 0.97 | |
| 17 ^[a] | TiO ₂ -[{Ru ^{II} (trpy)} ₂ (μ-((O-Phen)Ru ^{II} (dcbpy) ₂) ₂ bpp)(μ-PhCOO)] ⁵⁺ | TiO ₂ -18a | 0.79 | 1.15 | | 1.56 |
| 18 ^[b] | TiO ₂ -[{Ru ^{II} (trpy)} ₂ (μ-((O-Phen)Ru ^{II} (dcbpy) ₂) ₂ bpp)(H ₂ O) ₂] ⁶⁺ | TiO ₂ -18b | 0.55 | 0.78 | 0.86 | 1.33 |

[a] CV in 0.1 M TBAH in DCM. [b] CV in water pH = 1, triflic acid. [c] CV in 80:20 0.1M water pH = 1, triflic acid: TFE. [d] CV in 0.1M TBAH in Methanol. [e] CV in 1:1 0.1 M TBAH in DCM/TFE.

This catalytic wave is the major difference between the anchored aquo-complexes and their homogeneous counterparts: For FTO- TiO_2 -**12b**, the electrocatalytic wave observed for **12b**⁻ is no longer observed for the anchored catalyst but the multiple peaks for the PCET processes are still evident (Table 1 entries 5 and 14, and Figure 3f). Similar behaviour is also observed when one compares FTO- TiO_2 -**14b** and the equivalent unanchored complex **13b**, the bridging ligand is easily hydrolysed to give the bis-aquo moiety but there is no onset of catalysis before the baseline CV measurements for blank FTO- TiO_2 (Table 1 entries 8 and 16, and Figure 3g). Compound **18b** on the other hand, once anchored on FTO- TiO_2 , retained its catalytic activity and a large current increase over and above the blank electrode can be seen in Figure 3h for the FTO- TiO_2 -**18b** electrode.

The electrochemical data of all the ruthenium compounds investigated by CV and DPV, as well as the solvents employed and the $E_{1/2}$ potentials, are summarized in Table 1.

Water oxidation activity. In order to corroborate and quantify the observed electrocatalytic activity for the three complexes, CPE measurements were performed on the three supported catalysts. In the case of modified electrodes FTO- TiO_2 -**12b** and FTO- TiO_2 -**14b** they needed to be scanned up to 1.5 V (vs. SSCE) to observe what appears to be the beginning of an electrocatalytic process (see Figure 3g) therefore a potential of 1.6 V was chosen for the comparative CPE measurements. As expected, a significant increase in charge against time was only measured during the CPE measurement with the FTO- TiO_2 -**18b** electrode (see Figure

4). When the FTO-TiO₂-**12b** electrode was used, total detachment of the complex from the electrode surface was observed after 20 min. That makes the charge recorded during CPE not comparable with that of the other two electrodes. This is corroborated by the UV-vis analysis of the electrolyte from the anodic compartment (see ESI Figure S43). The results using FTO-TiO₂-**14b** as the anode showed no current above the blank over the course of the CPE experiment. However, in this case the leaching process was negligible and almost all the adsorbed catalyst **14b** remained attached to the TiO₂ after the CPE experiment (see ESI Figure S43).

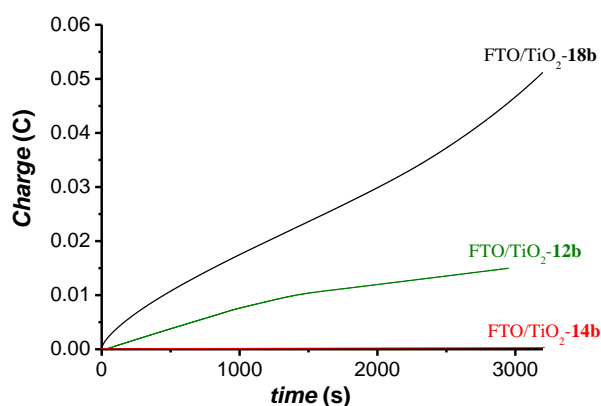


Figure 4. CPE experiments at pH=1 (0.1 M triflic acid aqueous solution) applying 1.6 V with the subtracted current of the blank using FTO/TiO₂-**18b** (black) and FTO/TiO₂-**14b** (red) as a working electrode, SSCE as reference electrode and platinum mesh as counter electrode. The CPE was carried out in a two compartment electrochemical cell (see ESI Figure S42), the anodic compartment contained the working and the reference electrode and the cathodic one the platinum mesh.

CPE experiments with the FTO-TiO₂-**18b** modified working electrode gave a charge of 0.05 C after 50 min of applied potential. This charge was attributed to oxidation of water to dioxygen after corroboration *via* analysis of the headspace with a Clark electrode (See Figure 5). Some leaching of the catalyst from the electrode during the CPE experiment was observed by UV-vis analysis of the anodic compartment afterwards, however, the majority of the material remained attached (see ESI Figure S43.) The relative stability of the anchoring groups in aqueous solutions is in agreement with observations made in previous reports in the literature,^[14] however, the different behaviour from an electrocatalytic perspective could not be related to the anchoring group only. For this purpose we turned into DFT to obtain a graphical representation of their structures anchored on TiO₂.

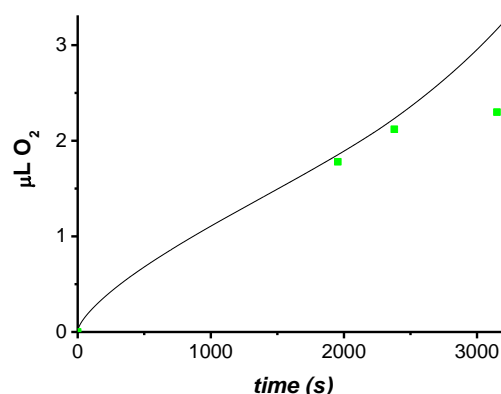


Figure 5. Oxygen generation measurement corresponding to the experiment presented in Figure 4 for FTO-TiO₂-**18b** based on (black) current vs. time analysis, and (green squares) a gas phase Clark electrode.

DFT Geometry optimization. The geometry of the complexes **12b**, **14b** and **18b** was optimized by DFT using the M06L functional including the solvent effects with the SMD model. The resulting structures were employed to estimate the dimensions of the cavity created by anchoring the complex onto the TiO₂ surface (see Figure 6), assuming a flat surface for TiO₂ as first approximation. This allowed to have a rough estimate of the cavity size between the anchored complex and TiO₂ as presented in Figure 6. For example, a cavity size of 92.6 Å² was calculated for FTO-TiO₂-**12b**, which provides more than enough room for extra water molecules around the catalyst active site given that the Van der Waals diameter of water is only 2.82 Å.^[15] The cavity size formed by adsorption of **14b** is drastically reduced to only 48.1 Å² and thus reduces the mobility of potential water molecules circulating within the cavity. This mobility is further decreased due to the cavity-inward situation of the Ru-aqua groups. Finally the cavity size formed for FTO-TiO₂-**18b** was calculated to be 182.8 Å², which is the largest of the three models. In addition, the catalyst active site is positioned outside of the cavity, which will also greatly increase its accessibility towards the substrate water molecules.

Based on the reactivity of these complexes it is clear that the catalyst orientation with regards to the surface plays a major role regarding its water oxidation capacity. Thus the *inward-facing*

catalysts, FTO-TiO₂-**12b** and FTO-TiO₂-**14b**, present no activity whereas the *outward-facing* catalyst FTO-TiO₂-**18b** is active. In addition the hydrophobic nature of the electrodes can also play a role preventing easy access of water for the *inward-facing* catalysts but would not affect the *outward-facing* catalyst. At this point it is worthwhile noting that although the previously reported examples of a pyrrole-trpy-modified Ru-bpp^[7] and pyridinium-trpy-

modified Ru-bpp^[9] showed catalytic activity after heterogenization, the anchoring process is different and results in a less ordered deposition with no fixed catalyst orientation with respect to the electrode surface.

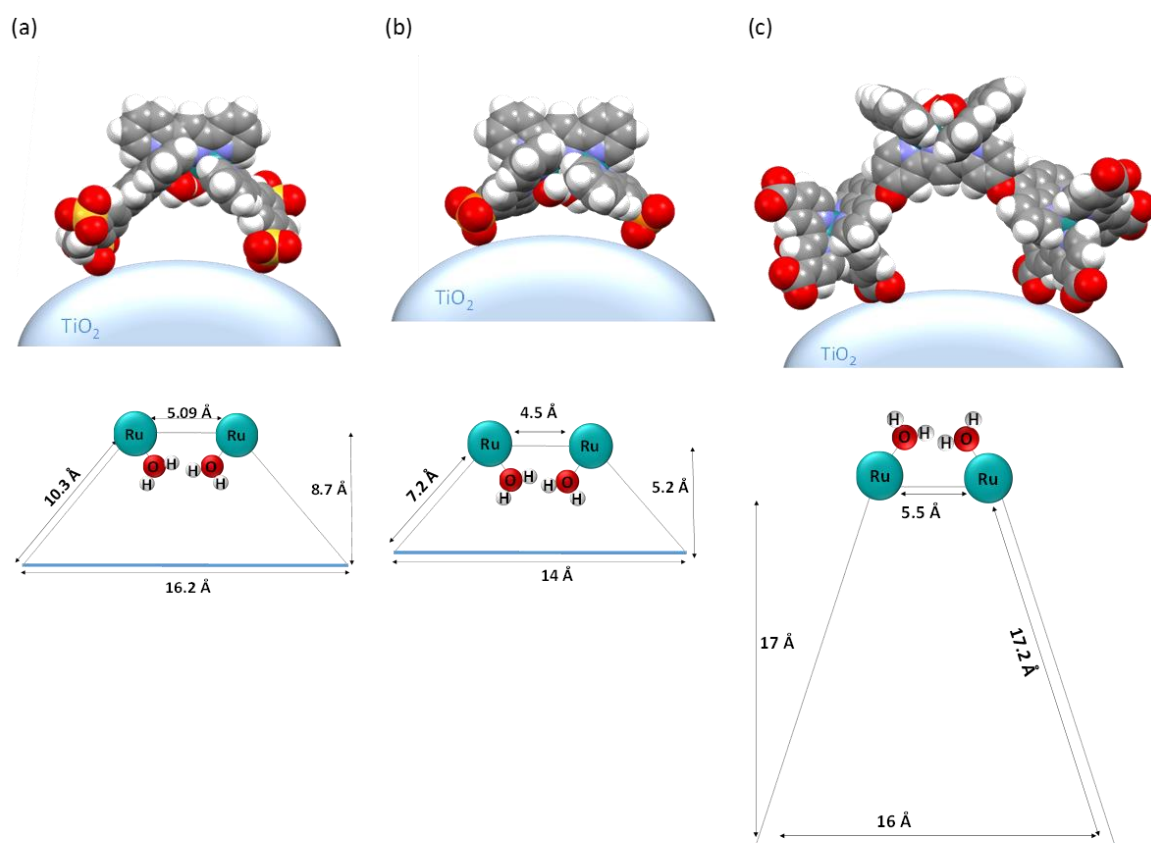


Figure 6. (Top) Van Der Waals sphere representation of the structures of the optimized geometry at the M06L DFT level of theory. Color code: O, red; S, orange; C, grey; H, white, Ru, green; N, blue. (Bottom) schematic representation of the most relevant approximate distances for complexes: (a) **12b**, (b) **14b** and (c) **18b**

Conclusions

In conclusion, three new compounds based on the Ru-bpp WOC have been synthesized and subsequently adsorbed onto mesoporous films of TiO₂ nanoparticles on FTO glass. The compounds all adsorbed onto the TiO₂ surface with different binding strengths, as expected due to the variation of the anchoring groups used; sulfonate, carboxylate and phosphonate. The catalysts all showed activity for electrocatalytic water oxidation when they were in a homogeneous solution however after anchoring on TiO₂ only compound **18b** retained its catalytic nature, the other two complexes were inhibited upon adsorption. Justification for the loss in activity was proposed to be due to the orientation of the catalyst active site with respect to the surface. DFT modelling of the free catalysts and their approximated anchoring on a flat TiO₂ surface showed the active site of compounds **12b** and **14b** to be enclosed within the cavity formed between the anchoring ligands and the TiO₂ surface. Compound **18b** importantly positioned the active site outside of the cavity and orientated away from the TiO₂ surface and thus allowed freer access for the water substrate. When designing functionalized Ru-bpp-catalysts, or similar catalysts with ≥ 2 anchoring groups for attachment to TiO₂, one should therefore pay strict attention to the positioning of the anchoring groups as well as their type and number in order to retain catalytic activity after anchoring. Following these recommendations, the optimum design would have a ligand modified with ≥ 2 aqueous-stable (phosphonate or hydroxamate) linkers with a binding geometry opposite to the active site to achieve strong catalyst-electrode binding and face the catalyst away from the electrode surface.

Acknowledgements ((optional))

We thank MINECO (CTQ-2013-49075-R, SEV-2013-0319; CTQ-2014-52974-REDC) and "La Caixa" foundation for financial support. COST actions, CM1202 and CM1205 from the EU are also gratefully acknowledged. CR thanks EU for a Marie Curie grant.

Keywords: Ruthenium • supported catalysts • water oxidation catalysis, water splitting • redox chemistry • organic-inorganic hybrid materials

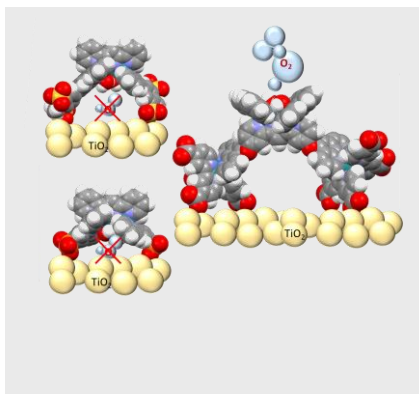
FULL PAPER

Entry for the Table of Contents (Please choose one layout)

Layout 1:

FULL PAPER

Text for Table of Contents



*Laia Francàs, Craig Richmond, Pablo Garrido, Nora Planas, Stephan Roeser, Jordi Benet-Buchholz, Lluís Escriche, Xavier Sala, Antoni Llobet **

Page No. – Page No.

Ru-bpp-based Water Oxidation Catalysts Anchored on TiO₂: The Importance of the Nature and Position of the Anchoring Group

- [1] S. Berardi, S. Drouet, L. Francas, C. Gimbert-Surinach, M. Guttentag, C. Richmond, T. Stoll and A. Llobet, *Chem. Soc. Rev.* **2014**, 43, 7501-7519.
- [2] (a) K. Fan, F. Li, L. Wang, Q. Daniel, E. Gabrielsson and L. Sun, *Phys. Chem. Chem. Phys.* **2014**, 16, 25234-25240. (b) P. Bornoz, F. F. Abdi, S. D. Tilley, B. Dam, R. van de Krol, M. Graetzel and K. Sivula, *J. Phys. Chem. C* **2014**, 118, 16959-16966. (c) L. Tong, A. Iwase, A. Nattestad, U. Bach, M. Weidelener, G. Gotz, A. Mishra, P. Bauerle, R. Amal, G. G. Wallace and A. J. Mozer, *Energy Environ. Sci.* **2012**, 5, 9472-9475.
- [3] (a) X. Li, J. Yu, J. Low, Y. Fang, J. Xiao and X. Chen, *J. Mater. Chem. A* **2015**, 3, 2485-2534. (b) M. de Respinis, K. S. Joya, H. J. M. De Groot, F. D'Souza, W. A. Smith, R. van de Krol and B. Dam, *J. Phys. Chem. C* **2015**, 119, 7275-7281. (c) C. D. Windle, E. Pastor, A. Reynal, A. C. Whitwood, Y. Vaynzof, J. R. Durrant, R. N. Perutz and E. Reisner, *Chem. Eur. J.* **2015**, 21, 3746-3754. (d) M. Schreier, P. Gao, M. T. Mayer, J. Luo, T. Moehl, M. K. Nazeeruddin, S. D. Tilley and M. Graetzel, *Energy Environ. Sci.* **2015**, 8, 855-861. (e) M. Haro, C. Solis, G. Molina, L. Otero, J. Bisquert, S. Gimenez and A. Guerrero, *J. Phys. Chem. C* **2015**, 119, 6488-6494. (f) B. M. Klepser and B. M. Bartlett, *J. Am. Chem. Soc.* **2014**, 136, 1694-1697. (g) E. Pastor, F. M. Pesci, A. Reynal, A. D. Handoko, M. Guo, X. An, A. J. Cowan, D. R. Klug, J. R. Durrant and J. Tang, *Phys. Chem. Chem. Phys.* **2014**, 16, 5922-5926. (h) C. Gimbert-Surinach, J. Albero, T. Stoll, J. Fortage, M.-N. Collomb, A. Deronzier, E. Palomares and A. Llobet, *J. Am. Chem. Soc.* **2014**, 136, 7655-7661. (i) D. Cedeno, A. Krawicz, P. Doak, M. Yu, J. B. Neaton and G. F. Moore, *J. Phys. Chem. Lett.* **2014**, 5, 3222-3226. (j) X. Chen, X. Ren, Z. Liu, L. Zhuang and J. Lu, *Electrochem. Commun.* **2013**, 27, 148-151. (k) Z. Ji, M. He, Z. Huang, U. Ozkan and Y. Wu, *J. Am. Chem. Soc.* **2013**, 135, 11696-11699. (l) T. Arai, S. Sato, T. Kajino and T. Morikawa, *Energy Environ. Sci.* **2013**, 6, 1274-1282. (m) L. Li, L. Duan, F. Wen, C. Li, M. Wang, A. Hagfeldt and L. Sun, *Chem. Comm.* **2012**, 48, 988-990. (n) C. D. Windle and R. N. Perutz, *Coord. Chem. Rev.* **2012**, 256, 2562-2570.
- [4] (a) L. Alibabaei, B. D. Sherman, M. R. Norris, M. K. Brennaman and T. J. Meyer, *Proc. Natl. Acad. Sci.* **2015**, 112, 5899-5902. (b) S. E. Bettis, D. M. Ryan, M. K. Gish, L. Alibabaei, T. J. Meyer, M. L. Waters and J. M. Papanikolas, *J. Phys. Chem. C* **2014**, 118, 6029-6037. (c) S. E. Bettis, K. Hanson, L. Wang, M. K. Gish, J. J. Concepcion, Z. Fang, T. J. Meyer and J. M. Papanikolas, *J. Phys. Chem. A* **2014**, 118, 10301-10308. (d) L. Zhang, Y. Gao, X. Ding, Z. Yu and L. Sun, *ChemSusChem* **2014**, 7, 2801-2804. (e) Y. Gao, X. Ding, J. Liu, L. Wang, Z. Lu, L. Li and L. Sun, *J. Am. Chem. Soc.* **2013**, 135, 4219-4222. (f) W. Song, A. Ito, R. A. Binstead, K. Hanson, H. Luo, M. K. Brennaman, J. J. Concepcion and T. J. Meyer, *J. Am. Chem. Soc.* **2013**, 135, 11587-11594. (g) L. Li, L. Duan, Y. Xu, M. Gorlov, A. Hagfeldt and L. Sun, *Chem. Comm.* **2010**, 46, 7307-7309. (h) W. J. Youngblood, S.-H. A. Lee, Y. Kobayashi, E. A. Hernandez-Pagan, P. G. Hoertz, T. A. Moore, A. L. Moore, D. Gust and T. E. Mallouk, *J. Am. Chem. Soc.* **2009**, 131, 926-927.
- [5] (a) J. T. Hyde, K. Hanson, A. K. Vannucci, A. M. Lapidus, L. Alibabaei, M. R. Norris, T. J. Meyer and D. P. Harrison, *ACS Appl. Mater. Interfaces* **2015**, 7, 9554-9562. (b) A. K. Vannucci, L. Alibabaei, M. D. Losego, J. J. Concepcion, B. Kalanyan, G. N. Parsons and T. J. Meyer, *Proc. Natl. Acad. Sci.* **2013**, 110, 20918-20922. (c) Z. Chen, J. J. Concepcion, J. F. Hull, P. G. Hoertz and T. J. Meyer, *Dalton Trans.* **2010**, 39, 6950-6952. (d) J. J. Concepcion, J. W. Jurss, P. G. Hoertz and T. J. Meyer, *Angew. Chem. Inter. Ed.* **2009**, 48, 9473-9476. (e) Z. Chen, J. J. Concepcion, J. W. Jurss and T. J. Meyer, *J. Am. Chem. Soc.* **2009**, 131, 15580-15581.
- [6] C. Sens, I. Romero, M. Rodríguez, A. Llobet, T. Parella and J. Benet-Buchholz, *J. Am. Chem. Soc.* **2004**, 126, 7798-7799.
- [7] J. Mola, E. Mas-Marza, X. Sala, I. Romero, M. Rodríguez, C. Viñas, T. Parella and A. Llobet, *Angew. Chem. Inter. Ed.* **2008**, 47, 5830-5832.
- [8] L. Francàs, X. Sala, J. Benet-Buchholz, L. Escriche and A. Llobet, *ChemSusChem* **2009**, 2, 321-329.
- [9] J. Aguiló, L. Francàs, H. J. Liu, R. Bofill, J. Garcia-Anton, J. Benet-Buchholz, A. Llobet, L. Escriche and X. Sala, *Catal. Sci. Tech.* **2014**, 4, 190-199.
- [10] L. Francàs, X. Sala, E. Escudero-Adán, J. Benet-Buchholz, L. Escriche and A. Llobet, *Inorg. Chem.* **2011**, 50, 2771-2781.
- [11] L. Mognon, J. Benet-Buchholz, S. M. W. Rahaman, C. Bo and A. Llobet, *Inorg. Chem.* **2014**, 53, 12407-12415.
- [12] A. Mishra, N. Pootrakulchote, M. K. R. Fischer, C. Klein, M. K. Nazeeruddin, S. M. Zakeeruddin, P. Bauerle and M. Graetzel, *Chem. Comm.* **2009**, 7146-7148.
- [13] F. Bozoglian, S. Romain, M. Z. Ertem, T. K. Todorova, C. Sens, J. Mola, M. Rodríguez, I. Romero, J. Benet-Buchholz, X. Fontrodona, C. J. Cramer, L. Gagliardi and A. Llobet, *J. Am. Chem. Soc.* **2009**, 131, 15176-15187.
- [14] (a) S. P. Pujari, L. Scheres, A. T. M. Marcellis and H. Zuilhof, *Angew. Chem. Inter. Ed.* **2014**, 53, 6322-6356. (b) J. Zhang, L. Sun, K. Ichinose, K. Funabiki and T. Yoshida, *Phys. Chem. Chem. Phys.* **2010**, 12, 10494-10502. (c) H. Park, E. Bae, J.-J. Lee, J. Park and W. Choi, *J. Phys. Chem. B* **2006**, 110, 8740-8749. (d) E. Bae, W. Choi, J. Park, H. S. Shin, S. B. Kim and J. S. Lee, *J. Phys. Chem. B* **2004**, 108, 14093-14101.
- [15] G. Graziano, *J. Chem. Soc., Faraday Trans.* **1998**, 94, 3345-3352